Pullulan-ionic liquid-based supercapacitor: A novel, smart combination of components for an easy-to-dispose device

Pullulan-based supercapacitor from biomass: a green solution for energy storage

Abstract

A pullulan-based supercapacitor featuring carbon electrodes obtained by the pyrolysis of pepper seeds and working with ionic liquid electrolyte is hereby proposed for the first time. Pullulan enables water processing of composite electrodes and the preparation of a bio-inspired separator by electrospinning. The supercapacitor delivers up to 5 kW kg^{-1} specific power and 25 Wh kg^{-1} specific energy at 3.2 V, therefore being comparable with conventional electrical double-layer capacitors and featuring the added value of being eco-friendly and cheap. The use of a water soluble, biodegradable polymer as binder and separator along with a hydrophobic ionic liquid brings about an easy-to-recycle device.

Keywords: green supercapacitor; pullulan; electrospinning; ionic liquid

Introduction

The skyrocketing demand for electricity and backup power for advanced transportation and most portable electronic devices has necessitated a great investment into energy research. Conversely, the environmental degradation accompanied with the routine generation of energy from fossil fuels for these applications has become a major concern. The replacement of these lethal energy generation techniques with renewable and green energy sources is wholly welcomed by researchers, consumers and stakeholders in the energy industry.

To fully exploit renewable energy sources, adequate storage systems capable of dealing with the inconsistent generation associated with most renewable energy sources are needed.

The limitations of the battery (Lithium and Sodium ion) systems with regards to the proper disposal methods is also seen as a drawback in the long term goal to attaining a cleaner and nontoxic environment [1,2]. Additionally, the high production and maintenance costs, low power density and poor cycle life for instant high power-demand and long-term applications makes them less favourable.

Supercapacitors, on the other hand, are potential storage systems which have been recently employed to complement battery systems and to be adopted as stand-alone backup units in more complex systems. With the numerous advancements being made in the supercapacitor field by researchers to solve the drawback on the low energy density, they are proposed as the next generation future storage technology for advanced applications due to their high-power capability, long cycle life and low maintenance costs.

The steps required to successfully design efficient supercapacitors lie in the development of sustainable electrode materials and electrolytes which are electrochemically active, environmentally benign (green), relatively low cost, recyclable and easily degradable. The focus on the electrode materials and electrolytes is due to the fact that they are the key parameters which determine

supercapacitor performance metrics (i.e. capacitance, operating voltage, stability, high specific energy and power) [3].

Recently, the use of activated carbon from biological waste (biochar) as a means of obtaining abundant low-cost materials was reported [4–9]. In this way, it is possible to design the pore structure of these porous materials to fit a specific electrolyte for effective "electrolyte ion – pore interaction"[10,11]. Some other reports have further incorporated the porous carbon with other materials to form hybrid composite materials to fully explore the different capacitance and operating potential windows values necessary in attaining high energy densities without losing on the power density [12,13]. Other studies have been focused on developing suitable conductive electrolytes which permits the electrode material to operate at largest achievable potential ranges [14–16]. Although the use of organic electrolytes has been extensively adopted in commercial supercapacitors, the instability in air and flammability can still be issues to contend with. Aqueous electrolytes on the other hand are limited to operation at a threshold voltage of 1.2 V due to the water present in them, but in some specific cases, operating voltages as high as 2.2 V have been achieved [16]. Moreover, organic and aqueous electrolytes cannot be used in high temperature applications due to the flammability and low boiling point temperatures respectively. Ionic liquids (ILs) provide the solution to the problems associated with organic and aqueous electrolytes but are saddled with low ionic conductivities and high costs. Thus, a trade-in on the cost of other less crucial components (such as separator, binders, current collectors) as compared to specific key elements could compensate for the overall cost. In fact, it is well known that most of the synthetic binders are harmful during the end-life disposal of these device [3].

Thus, the increased need for batteries and supercapacitors will mean large end-of-life waste. Strategies that lower the environmental and economic impact of disassembly and recycling of waste devices are thus mandatory [2].

In this context, the use of water-processable electrode binders and new membrane production techniques capable of exploiting natural and bio-inspired polymers, are a viable approach to decrease the cost and environmental footprint of the current productive processes.

Water-processable binders (e.g. carboxymethyl cellulose, alginate) are relatively cheaper options for use and improve the environmental compatibility of the electrode preparation process. They represent an emerging viable alternative in place of much more expensive fluorinated polymers like polytetrafluoroethylene and polyvinylidene difluoride that even require solubilization in a toxic N-Methyl-2-pyrrolidone solvent [17].

Pullulan is a biodegradable polysaccharide-based biopolymer. It is obtained from starch by the fungal species *Aureobasidium pullulan* [18] Pullulan films exhibit high solubility in water. Their transparency flexibility and low permeability to oxygen make them ideal packaging materials for food, pharmaceutical, and biomedical applications [19,20].

The present study involves the design and assembly of a pullulan-based electrical double layer capacitors (EDLCs) using biomass derived activated carbon prepared from a facile and environmentally safe technique with a mild activating agent. Pepper seed waste was used as carbon precursor and potassium hydrogen carbonate served as the activating agent.

The suitable electrode processing from polysaccharide polymer-containing slurries and an electrospun pullulan separator was adopted in a bid to reduce cost and also the inclusion of toxic fluoride-based binders. The use of pullulan as a key component for the development of green supercapacitors is herein reported for the first time. Specifically, pullulan is adopted as both water-processable binder and an electrospun separator. Electrospinning is an emerging technology for the preparation of controlled diameter fibres ranging from tens of nanometres to few micrometres. In recent years it has been considered as a promising process for the preparation of free-standing fiber mats to be used as electrode materials and separators in supercapacitors [21].

The pullulan-based EDLC featured 1-ethyl-3-methylimidazolium bis(trifluoromethylsulfonyl)imide (EMIMTFSI) as electrolyte. The choice of this IL is driven by its good ionic conductivity matched with a wide electrochemical stability enabling EDLCs to operate at voltages even greater than 3 V. Furthermore, EMITFSI is a hydrophobic electrolyte and this peculiar characteristic permits the design of a smart process to manage pullulan-based EDLC waste disposal. This concept is described in Scheme 1. The Scheme shows that at the end-of-life, the pullulan-IL-based EDLC can be simply separated in each of its components by immersion in water. Pullulan binder and separator are dissolved in water. Simultaneously a physical separation of the carbon powder, the hydrophobic IL, the current collector and the aqueous solution containing the biodegradable biopolymer takes place. The carbon powder and current collector can be recovered from the IL by filtration. Thus, the carbon material, current collector and IL could be recycled. The pullulan aqueous solution is biodegradable and can be disposed without any negative impact on the environment.

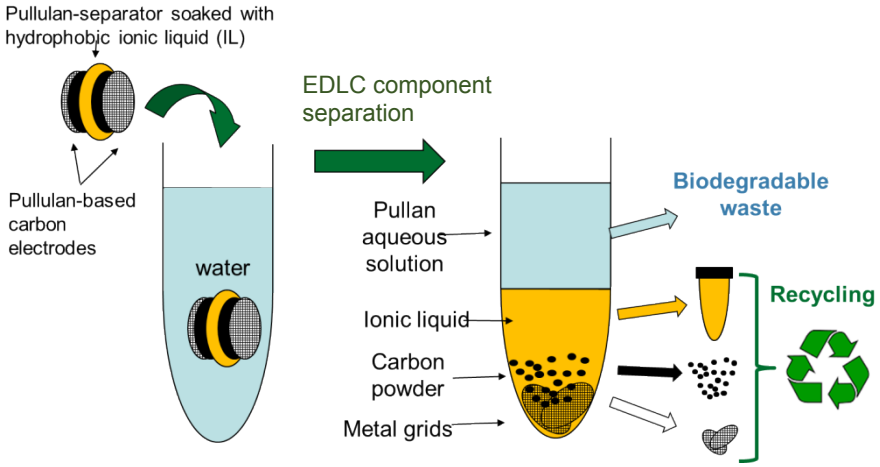

Scheme 1. Concept of pullulan- and IL- based EDLC waste management.

Experimental

The synthesis of the porous carbon PP-AC is as described in our earlier work [22]. Briefly, the seeds were obtained as waste from cheap Bell peppers. They were thoroughly mixed with potassium hydrogen carbonate ($KHCO_3$) (serving as the activating agent) in a mass ratio of 1:1 to obtain a homogenous mixture.

Compactivation of the final mixture into a rectangular mould was done by adding little deionized water to the powder in an agate mortar before drying in an oven at 80 °C for 6 h to remove the water. The dried mould was placed in a furnace purged with a regulated flow of argon gas (250 sccm) at a 5 °C min^{-1} ramp rate for 2.8 h to an 850 °C final temperature. The carbonization process was run for a 2 h period with subsequent cooling to 25 °C. The final product was sonicated for 0.5 h, washed with 3 M HCl and rigorously rinsed with deionized water to attain a neutral pH. The complete chemical and physical characterization of the PP-AC carbon is reported in the earlier work [22].

The reference material, a commercial carbon ACT (PICA) was treated at 1050 °C in Ar for 2 h, before use. This treatment was performed to clean the carbon surface from oxygen- and nitrogen-moieties produced after activation [23]. While surface cleaning improves carbon wettability with the hydrophobic IL, it also permits a better comparison with the PP-AC carbon that was obtained by pyrolysis at high temperature under an inert atmosphere as the final synthesis step.

Nitrogen adsorption porosimetry measurements were carried out at 77 K with an ASAP 2020 system (Micromeritics) after a drying step for 24 h at 180 °C. The N_2 adsorption isotherms were analysed by density functional theory (DFT) to obtain the pores size distribution (PSD).

Electrodes were prepared by an aqueous process. In order to achieve an electrode composition of 70% PP-AC or ACT, 10 % Carbon black, 20 % binder, a slurry containing 24 mg of PP-AC or ACT, 3 mg of carbon black (as conducting additive), 3 mg of pullulan (P0978, TCI) and 3 mg of Glygerol (Sigma Aldrich), in 0.9 g of MilliQ water was casted on pre-cut Nickel foams (Alantum, Munich, Germany, diameter 0.9 cm). For electrodes having the composition 85% ACT, 5 % Carbon black, 10 % binder, the slurry contained 20.25 mg of ACT, 1.2 mg of carbon black (as conductive additive) and 1.14 mg of pullulan and 1.14 mg of glycerol in 0.28 g of Milli Q water. The slurry was deposited on the Nickel foam by drop casting and dried under vacuum into Büchi oven overnight at room temperature.

Electrodes were dried in a vacuum oven overnight at room temperature (büchi glass oven B-585). The composite electrode loading (excluding the Nickel foam mass) was in the range 4-7.5 mg cm^{-2}.

The home-made electrospinning apparatus consisted of a high-voltage power supply (Spellman SL 50 P 10/CE/230), a syringe pump (KD Scientific 200 series), a glass syringe containing the polymer solution and connected to a stainless-steel blunt-ended needle (inner diameter = 0.51 mm) through a PTFE tube. The pullulan membrane was electrospun using a 23% w/v solution of pullulan in Milli-Q water. The solution was spun at 18 kV at a distance of 20 cm from the collector with a flow rate of 0.9 mL/h. Electrospinning was performed at room temperature (RT) and a relative humidity of 40-50%. Scanning electron microscopy (SEM) images of the membrane was collected using a ZEISS EVO 50 apparatus.

Tensile stress–strain measurements were performed by using a Dynamic Mechanical Thermal Analyzer (DMTA, TA Instruments Q800 series) equipped with tension-film clamps. The analyses were performed on rectangular strips cut from the electrospun mat (width 5 mm; gauge length about 10 mm). Stress-strain measurements were carried out at room temperature by applying a preload force of 0.01 N and using a cross-head speed of 5 mm/min. Six rectangular specimens were analysed for each sample. The specimen thickness (about 0.1 mm), measured with a digital micro-meter, was used to obtain stress-strain curves from raw load-displacement data.

Stress and strain at yield (σ_y and ε_y), stress and strain at break (σ_b and ε_b) as well as the tensile modulus (E) were determined as the average value ± standard deviation.

Supercapacitors were assembled from two carbon composite electrodes alienated by a circular sheet of electrospun pullulan separator, with 1-Ethyl-3-methylimidazolium bis(trifluoromethylsulfonyl)-imide IL (EMIMTFSI, Solvionic) as electrolyte. A T Swagelok-type cell assembly (BOLA Cell made from Teflon) with a silver quasi-reference electrode disk was used. Cells were assembled in a dry box (MBraun Labmaster 130, H_2O, and O_2 < 0.1 ppm). The separator and electrodes were

soaked under vacuum with the IL before the assembly. The total composite mass of the two electrodes (m_{EDLC}) was in the 9-14 mg cm^{-2} range. The positive to negative electrode composite loading ratio was > 1 to achieve cell voltages higher than 3 V [24,25].

The electrochemical tests were performed in a thermostatic oven at 30° using a BioLogic VSP multichannel potentiostat/galvanostat/FRA. Voltammograms where analysed to evaluate capacitance. Specifically, the capacitance values were obtained by the slope of the discharge voltammetric current integrated over time vs. electrode potential (or cell voltage for the 2-electrode case) plots. Values are normalized to the composite electrode mass.

Electrochemical impedance spectroscopy was performed with 100 kHz–100 mHz frequency range and 5 mV AC perturbation, acquiring 10 points per decade.

Results and Discussion

Carbon porosity is the main feature affecting electrode capacitance. Figure 1a shows the N_2 adsorption–desorption isotherms of the PP-AC and ACT carbons. At low pressures the adsorption-desorption branches illustrated narrow hysteresis loops which are indicative of type 1 isotherm and of materials containing micropores. However, at high relative pressure (p/p^0=0.45-0.9) the PP-AC and ACT carbons displayed type IV isotherm adsorption-desorption branches showing the existence of mesopores [26]. The isotherm analysis provided similar values of Brunauer–Emmett–Teller (BET) specific surface area for the two carbons, namely 1990 $m^2\ g^{-1}$ and 1960 $m^2\ g^{-1}$ for PP-AC and ACT. The DFT plots confirmed the presence of micropores and mesopores in both carbons that however are distributed differently [27].~~This suggests that the porosity originated by the smallest pores is similar for the two carbons~~. Figure 1b reports the specific incremental pore volume distributions. The PP-AC carbon feature bimodal pore distribution centered at 0.8 nm and 2.5 nm. The ACT carbon has the majority of the pores featuring a width of 2.5 nm. Unlike PP-AC, ACT displays a not-negligible mesoporosity coming from 4-11 nm pores, centered at 6 nm. Figure 1c

reports the cumulative volume of pores wider than 0.4 nm. The total pore volume is similar for the two carbons. However, for PP-AC the micropore volume (pores width <2 nm) contributes with higher extent to the porosity with respect to ACT. Indeed, the micropore volume is 0.56 $cm^3\ g^{-1}$ and 0.45 $cm^3\ g^{-1}$ for PP-AC and ACT, corresponding to 59.6 % and 36.7 % of the total volume ($V_{>0.4\ nm}$) respectively.

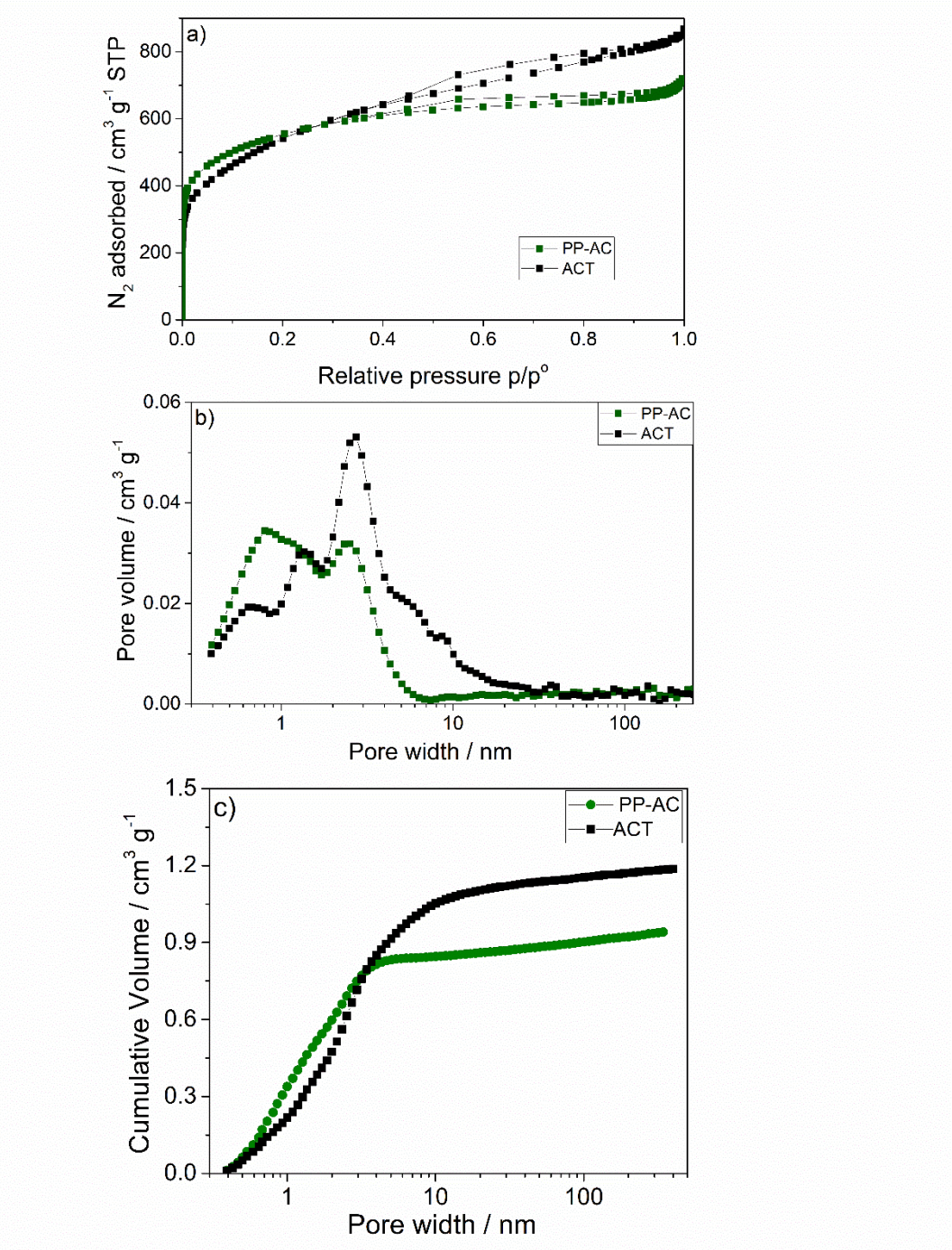

Figure1. (a) N_2 adsorption-desorption isotherms in the p/p_0 range 2.95 10^{-7} to 0.999 and DFT b) incremental and c) cumulative pore volume vs. pore size of the PP-AC and ACT carbons.

The pore size distribution of the two carbons ~~perfectly~~ fits with the requirement for use in IL-based supercapacitors. Indeed, in order to avoid electrolyte starving effects that cause limitations in charge storage capability, carbon pores should be wider than the IL-ion size. For EMITFISI, the largest ion dimension has been estimated to be ca. 0.8 nm [24,28,29,30]. Table 1 summarizes the main porosity features of the PP-AC and ACT carbons along with the Raman I_D/I_G ratio of the D-band and G-band intensities. The lower I_D/I_G ratio of PP-AC indicates a higher graphitic domain fraction with respect to ACT.

Table 1. BET surface area (S_{BET}), DFT specific pore volume from pores with size > 0.4 nm ($V_{>0.4\ nm}$) of the PP-AC and ACT and specific capacitance (C_{carbon}) of the carbons from CVs at 40 mVs^{-1} in EMIMTFSI (average of the values of the positive and negative electrodes and normalized to the high surface area carbons, (i.e. excluding carbon black and binder). I_D/I_G is the ration of the Raman D-band and G-band intensities from [22, 23].

Carbon	Code	S_{BET} /m^2g^{-1}	$V_{>0.4\ nm}$ /cm^3g^{-1}	C_{carbon}/Fg^{-1}	I_D/I_G
Pepper-derived	PP-AC	1990	0.94	115	0.96
Commercial	ACT	1960	1.19	75	1.09

The other chemical and physical properties of the PP-AC carbon are as summarized below based on the characterization reported previously by Momodu et al. [22]. The PP-AC carbons displayed a porous carbon network morphology as observed from the SEM and TEM images [22]. The powder X-ray diffraction analysis of the PP- AC showed broad peaks at 26˚ and 43˚ that are attributed to the 002 and 100 planes of graphite structure in amorphous carbon material. Prior Raman analysis indicated the presence of typical D and G bands at 1344 cm^{-1} and 1594 cm^{-1}, respectively. These were associated with the presence of sp^3-induced defects and sp^2 carbon domains[22,31]. Moreover, the presence of lattice distortions due to edge defects and sp^2-sp^3 bonds was evidenced by the presence of an additional D* shoulder at 1203 cm^{-1}[32].

The elemental composition of the PP-AC was determined using X-ray Photoelectron Spectroscopy (XPS). The survey scans showed two distinct peaks corresponding to C1s (284 eV) and O1s (532 eV). The deconvolution of the high-resolution XPS signal of C1s, displayed the main component peak (~ 284.6 eV) corresponding to the sp^2 C=C bonds [33], whereas the peak located at ~288.8 eV and ~285.9 eV were ascribed to the presence of C=O and C-O-C bonds [34], respectively. Finally, the O1s spectrum gave degenerate peaks associated with C=O (~ 532 eV) and O-C (~ 533.4 eV) [35]".

Pullulan is a highly water-soluble polymer that makes it of interest as binder for water-processable electrodes. However, the brittleness of pullulan films requires blending with plasticizers to improve the mechanical properties of pullulan-based films. In references [19,20], it is reported that glycerol is a suitable plasticizer. Indeed, pullulan-glycerol films casted from aqueous solution with glycerol concentration of 20-30% w/w featured physical-mechanical properties acceptable for pharmaceutical and food packaging applications. This can be visually appreciated in Figure 2a that shows a stretchable self-standing transparent film which is easily peeled-off from the Petri plate. We, therefore, used a blend of pullulan and glycerol as binder of supercapacitor carbon electrodes. In our study, the best adhesion of the carbon layer to the current collector was achieved by mixing pullulan and glycerol with a 1:1 wt. ratio. Figure 2b shows the image of a carbon electrode obtained by casting a layer based on 70% high surface carbon - 10% conductive carbon - 20% pullulan-glycerol (1:1 wt.) on nickel foam.

An additional strategy that can be adopted to process biopolymers film is electrospinning. This method enables to obtain non-woven mats composed of interconnected fibers that can be used as separators. Figure 2c and 2d report the images of the electrospun pullulan film that was used to assemble the green supercapacitors. The mat thickness was 55 µm with defect-free fibers with a 0.34 µm diameter.

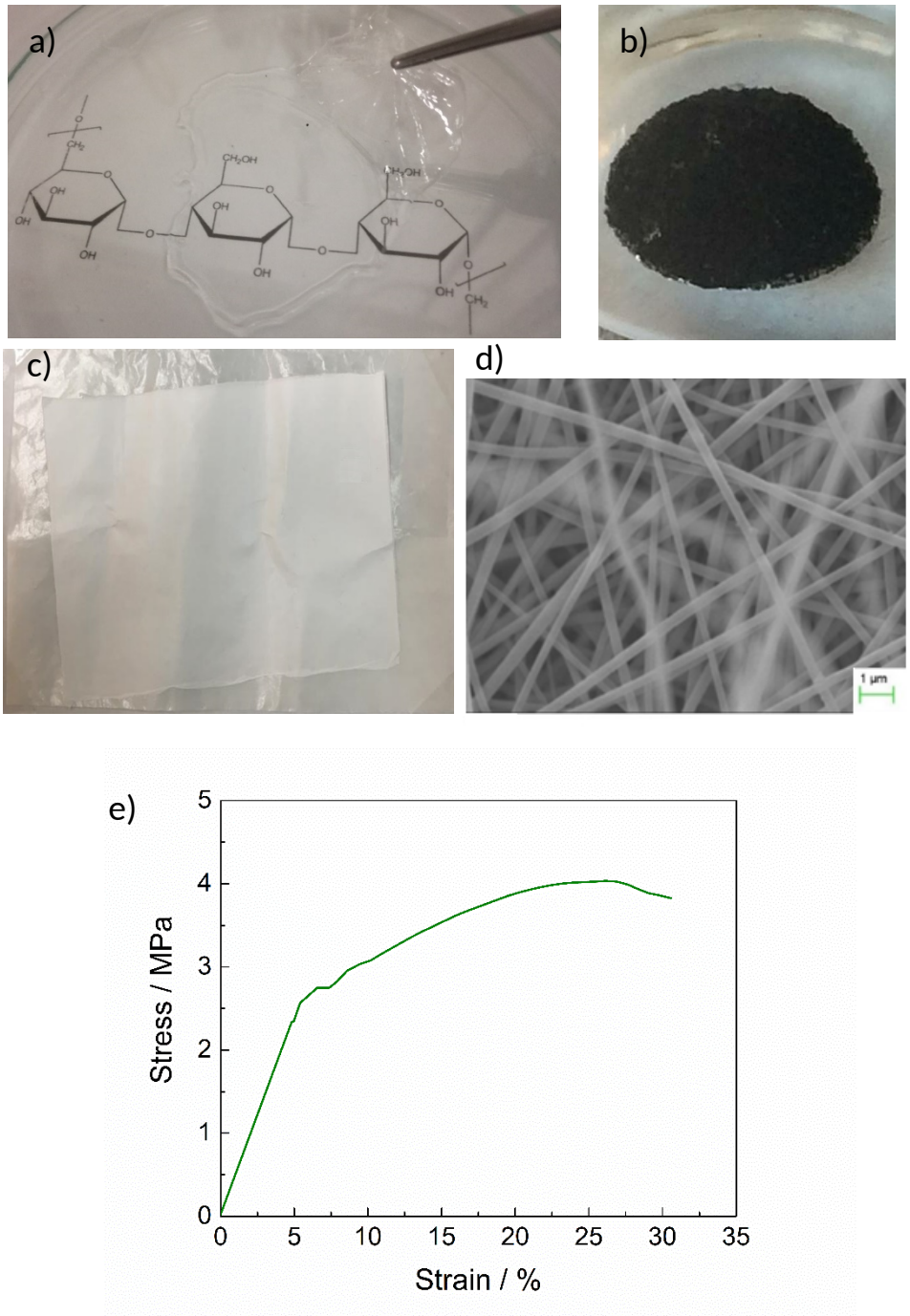

Figure 2. a) pullulan-glycerol film obtained by drying at 60 ˚C a casted layer of 100 mg pullulan – 30 mg glycerol in ca. 1.5 g of water.; b) carbon electrode prepared by casting an aqueous ink with carbon powder, pullulan and glycerol on nickel foam; c) picture and d) SEM image of the electrospun pullulan separator and e) Stress-strain curve of pullulan electrospun mat.

Tensile stress-strain measurements were run for pullulan electrospun fibre mats. Figure 2e displays a representative stress-strain curve for the fibre mat, from which mechanical properties data were

calculated. The mat showed an elastic modulus E = 85±27 MPa, a stress at break σ_b = 3.4±0.4 MPa and a strain at break ε_b = 32±9 %.

It is known that fibre arrangement in the mat usually changes in the course of a stress–strain analysis. Fibres tend to align in the direction of the applied force before getting thinner and finally breaking [36]. The complex phenomena of fiber rearrangement that occurs during scaffold deformation might explain the high variability of mechanical data that is often found when analysing electrospun mats.

The pullulan-based electrodes were tested by cyclic voltammetry in both three- and two-electrode cell setup. Figure 3a and 3b show the voltammograms of single electrodes at 40 mV/s. The profile of the voltammograms approaches the box-shape expected for EDLC electrodes. The Figures 3a and 3b also demonstrate that within the potential range from +1.4 V to -1.4 V vs Ag, additional signatures eventually related to side reactions that can be ascribed to pullulan are not evident. This is a first indication of the good compatibility of pullulan with EMIMTFSI.

From the analysis of the voltammograms of Figures 3a and 3b, the specific capacitance of PP-AC and ACT composite electrodes in the positive domain are 70 F g^{-1} and 45 F g^{-1}, respectively. For the negative domain the specific capacitance of PP-AC is 90 F g^{-1} and that of ACT is 60 F g^{-1}. The specific capacitance averaged on the positive and negative domains and normalized only to the mass of the high surface area carbons (excluding carbon black and binder) is 115 F g^{-1} and 75 F g^{-1} (Table 1) for the PP-AC and ACT. ~~This proves that, despite a lower specific surface area and porous volume (see Figure 1 and Table 1), the biomass derived activated carbon overcomes the performance of the commercial carbon ACT.~~

The PP-AC capacitive response well compares to that featured by electrodes produced with the same carbon, the same electrolyte but with a PVdF binder (20%) [22]. These electrodes featured specific capacitance of 116 F g^{-1} at 1 A g^{-1}.

For most practical applications, the volumetric capacitance should be taken in account. The electrodes investigated here featured a porous Nickel foam current collector that mainly contributed to the electrode volume with a thickness of 270 μm. Therefore, while electrode specific capacitance was of interest for supercapacitor application, the volumetric capacitance was low.

~~This is not surprising because, even in the condition that carbon pores are wide enough to accommodate ions, like in our case, the gravimetric capacity might not linearly increase with the meso-macropore surface area. Indeed, space charge capacitance in the pore walls, that decreases with pore wall thickness, plays a role in the different capacitive response of the electrodes [23,24,27,28, 29,30]. Pore walls thinner than 2–3 times of the pore wall screening length (0.3-0.4 nm) would account for a charge storage limitation in the solid part of the carbon/IL interface.~~

~~Table 1 shows that the pore volume of the ACT (0.72 $cm^3 g^{-1}$) is 40% greater than PP-AC's (0.42 $cm^3 g^{-1}$). Consequently, it is reasonable to assume that ACT pore walls are thinner than those of PP-AC. On the basis of geometric considerations, we reported that ACT pore walls might have an average thickness in the order of few graphene layers that is close to the screening length of the electric field in the carbon [27]. Therefore, the lower specific capacitance of ACT with respect to PP-AC can be explained with a lower space charge capacitance that negatively impacts on the global capacitive response of the electrode. Hence, PP-AC features an optimal porosity for a use in IL-based supercapacitors.~~

~~In agreement with reports in literature [24], for both carbons the potential range of the negative electrode is wider than the one of the positive in EMITFSI. Hence, in order to exploit the whole electrochemical stability of EMITFSI, the positive electrode should feature higher mass with respect to the negative.~~ Figures 3c and 3d report the 2-electrode voltammograms of the PP-AC and ACT based EDLCs at 5 mV s^{-1} and 200 mV s^{-1} scan rates up to a cell voltage as high as 3.2 V. At the lowest scan rate the coulombic efficiencies is 89 % for ACT-EDLC and 92 % for PP-AC-EDLC. Efficiencies increase to 98.3 % and 99.5 %, respectively, at 200 mV s^{-1}.

Notably, the voltammograms keep a symmetric, box-like shape even at high scan rate up to 200 mV s^{-1}. At this scan rate the specific currents (evaluated considering the total composite mass loading of the two electrodes, m_{EDLC}) approach a high value of ~ 4 mA mg^{-1}.

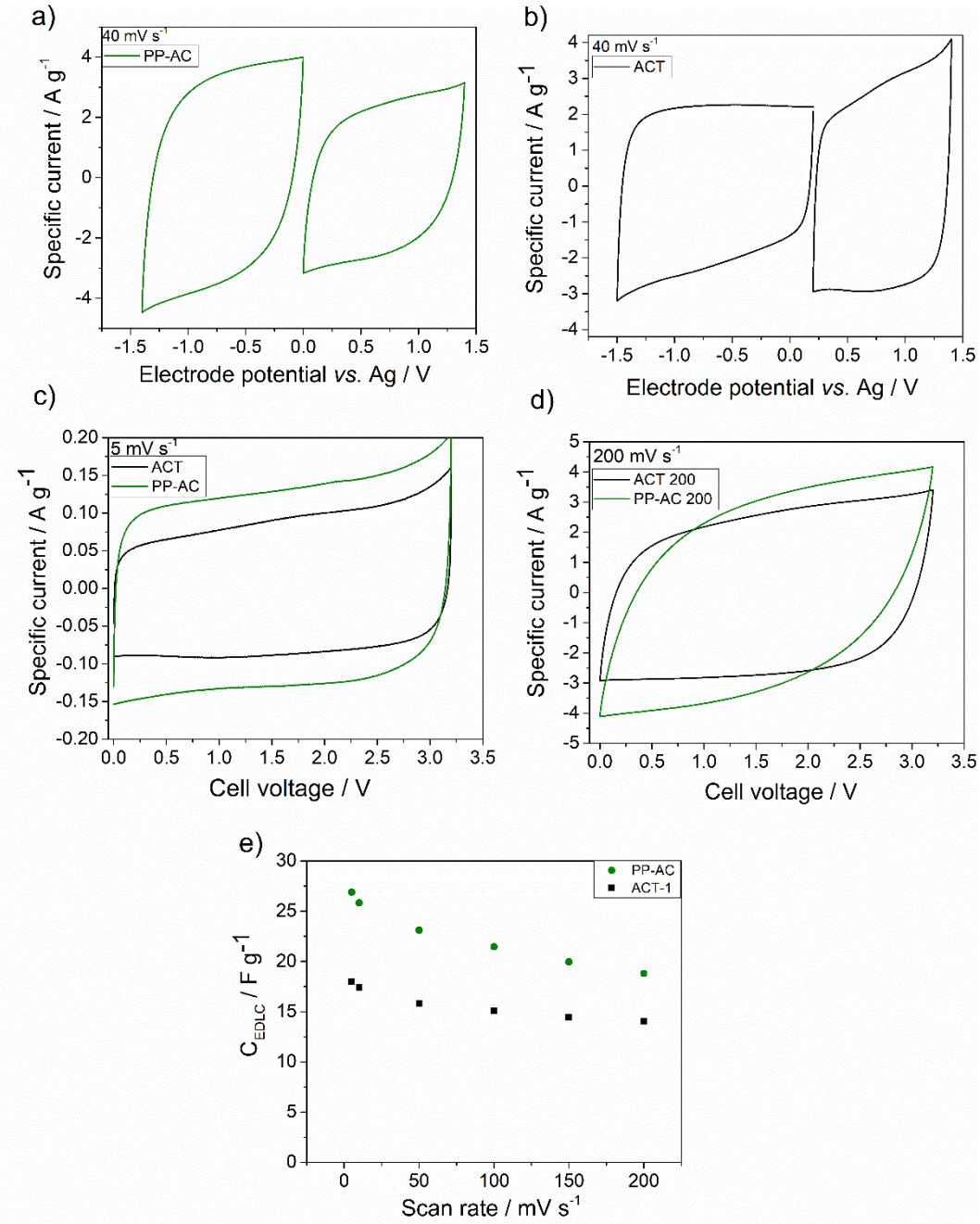

Figure 3. Three-electrode voltammograms of a) PP-AC and b) ACT electrodes at 40 mV s^{-1}, two-electrodes voltammograms of PP-AC and ACT at c) 5 mV s^{-1} and d) 200 mV s^{-1}, and e) trend of the supercapacitor specific capacitance (C_{EDLC}) vs. the scan rate.

The voltammetric capacitance retention with the increase of the scan rate evaluated from the cycles shown in Figures 3c and 3d is reported in Figure 3e. At each scan rate, the specific capacitance of

the supercapacitor featuring PP-AC is greater than that of the supercapacitor with ACT. This is in agreement with the higher specific capacitance of PP-AC electrodes evaluated by three-electrode CVs.

Despite Raman analyses provided indications of a lower degree of graphitization for ACT (Table 1), the ACT capacitance retention with the increase of the scan rate lower than that of PP-AC-EDLC (30%). The ACT capacitance decreased by 22% from 5 mV s^{-1} to 200 mV s^{-1}, while the PP-AC's reduced by 33%. The best capacitance retention of the former carbon can be explained referring to its pore distribution (Figure 1b). The biomass-derived activated carbon has a higher volume from pores narrower than 2nm with respect to ACT. On the contrary, ACT has an additional distribution in the range of 5-15 nm that enables a better ionic connection between the disordered pores and an easier access of ions to the carbon surface for the double-layer charge/discharge.

The effect of the different porous architecture of the two carbons on their electrochemical performance is further supported by the Nyquist plots reported in Figure 4. The plots have been obtained from EIS analysis carried out in 2-electrode setup and represent the impedance of the PP-AC-EDLC and ACT-EDLC. The slope of the low-frequency part of the plots is lower for PP-AC-EDLC and this is related to a slower diffusion of ions into the carbon pores with respect to ACT.

The high frequency resistance (intercept on the real axis) includes ionic and electronic terms related to EMITFSI resistivity through the pullulan separator and to the electrode contact resistances. The high frequency resistance of PP-AC-EDLC is 2.7 Ω cm^2 and half that of ACT (5.2 Ω cm^2), despite that higher mass loading used in the former EDLC. The total composite electrode mass loadings were 11.6 mg cm^{-2} and 9.3 mg cm^{-2} for PP-AC-EDLC and ACT-EDLC, respectively. Note that an EDLC featuring EMITFSI and PP-AC electrodes with PVdF binder and Nickel foam current collector exhibited a much higher ESR of 20 Ω cm^2 [22]. This indicates that pullulan effectively binds the carbon powders on the nickel foam current collectors. Figure 4a also demonstrates that the pullulan electrospun separator can be used to assemble low equivalent series resistance (ESR)

EDLCs.

Figure 4b reports the Nyquist plots of symmetric cells with stainless steel blocking electrodes separated by the Pullulan membrane used in this work or a commercial membrane (Whatman GF/A, fibre glass) soaked in EMIMTFSI. The intercept on the Real axis of the Nyquist plot at the highest frequency (500 kHz) is representative of the ionic resistance through the membrane. For the Pullulan membrane the resistance was 1.8 Ω cm^2 and well compared with that of the commercial separator that feature 2.1 Ω cm^2. These results even permit to evaluate that the electrode contribution to the PP-AC-EDLC ESR is less than 1.4 Ω cm^2 and 0.8 Ω cm^2 for the ACT-EDLC.

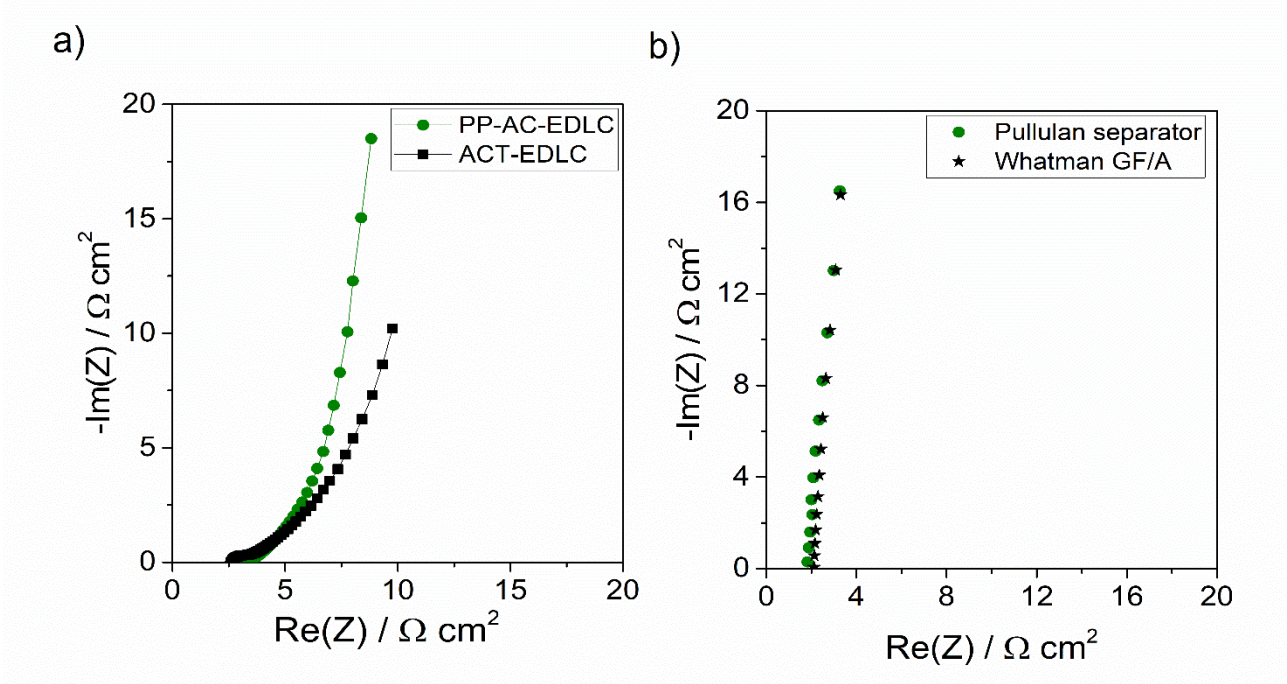

Figure 4 Nyquist plots of: a) the PP-AC and ACT based EDLCs (two-electrode setup, frequency range: 100 kHz to 10 mHz). The total composite electrode mass loadings were 11.6 mg cm^{-2} and 9.3 mg cm^{-2} for PP-AC-EDLC and ACT-EDLC; b) symmetric cells with stainless steel blocking electrodes separated by the Pullulan membrane used in this work or a commercial membrane (Whatman GF/A, fibre glass) soaked in EMIMTFSI (frequency range from 500 kHz to 15 kHz).

The feasibility of the use of pullulan binder was also investigated with electrodes featuring higher loadings and lower binder concentration. Specifically, we assembled an additional EDLC with electrodes having both the following composition: 85 % ACT, 5 % carbon conductive additive and 10% of binder. Hereafter, this EDLC is labelled ACT-EDLC-2. The cycling performance of the

pullulan-based EDLCs was evaluated by galvanostatic charge-discharge cycles at different specific currents. Figure 5a reports the cell voltage as a function of the time at different specific currents between 0 V and 3.2 V for the PP-AC- and the two ACT-based EDLCs. The charge/discharge profiles are symmetric, triangular shaped with linear voltage vs time profile. The coulombic efficiencies of the charge/discharge cycles of the three tested EDLC, reported in Figure 5 labels approach 100 % at the highest specific currents of 4-5 A g^{-1}.

These high specific currents can be achieved thanks to very low IR drop of the EDLC. Indeed, the use of pullulan as both a separator and binder enable IR drops of values of 0.14 V (at 1 A g^{-1}) for the PP-AC-EDLC, 0.08 V (at 1 A g^{-1}) for the ACT-EDLC and 0.21 V at (1 A g^{-1}) for the ACT-EDLC-2.

The discharge profiles reported in Figures 5a, 5b, 5c were analysed to build the Ragone plots reported in Figure 5d in terms of specific energy (E, in Wh kg^{-1}) and power (P, in kW kg^{-1}) which were calculated using Eqs. (1) and (2):

$$E = I \int V \cdot \frac{dt}{3600} \quad (1)$$

$$P = 3600 \cdot \frac{E}{\Delta t} \quad (2)$$

where I is the specific current (in A g^{-1}) and Δt is the discharge time (in s). The specific current is normalized to the total mass of composite material of the two electrodes.

At the highest specific current (4-5 A g^{-1}) the PP-AC and ACT EDLCs displayed 5 kW kg^{-1} and 8 kW kg^{-1}, respectively. The highest specific energy delivered at the lowest specific current (0.5 A g^{-1}) and was 25 Wh $kg^{-1}$and 20 Wh kg^{-1} for PP-AC and ACT EDLCs respectively. These values are within the same order of magnitude of those featured by lab-scale cells assembled with conventional electrodes and separator materials but had the great advantage of being obtained with

green (environmentally friendly) components. The highest specific energy featured by the PP-AC EDLC is due to its high specific capacitance discussed above. The ACT-EDLC-2 maximum specific power was 4 kW kg^{-1} with a maximum specific energy of 7 Wh kg^{-1}. In our opinion the reason is that in this cell the increase of the mass loading was paralleled by the decrease of the conductive additive percentage to 5 % (it was halved). This made the connection between the carbon particles and the current collector more difficult and ultimately to not fully exploit the electrode area for the energy storage process.

Finally, Figure 5e shows the trend of the capacitance normalized by the value featured at the first cycle under repeated cycles at 1 A g^{-1} of the three tested EDLCs. Despite the not optimized energy and power performance, the ACT-EDLC-2 cell featured very good stability proven over 5000 cycles. Hence, these preliminary results suggest that pullulan can be also effective in keeping a good cyclability of the EDLCs even when used as binder at percentage as low as 10%.

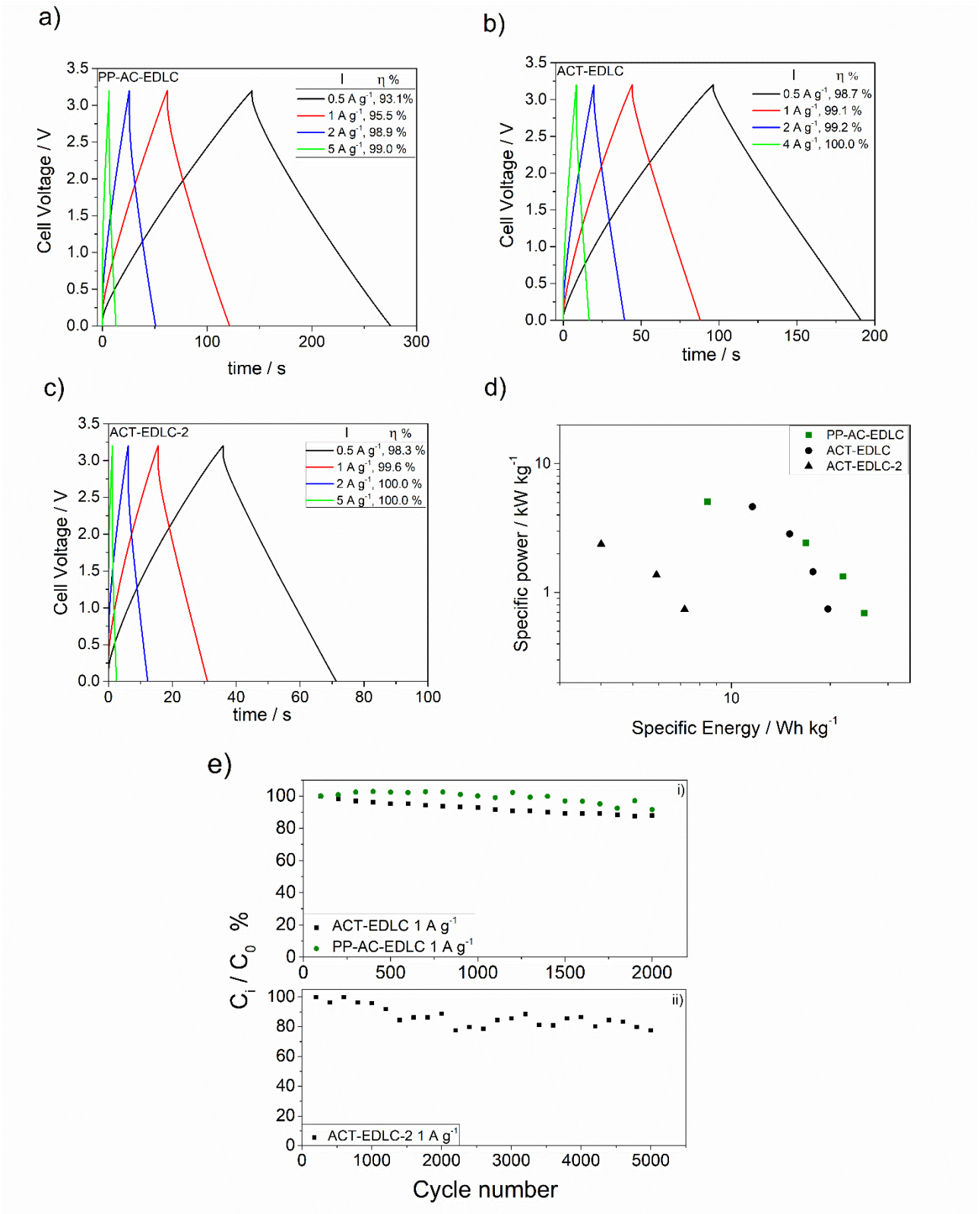

Figure 5. Cell voltage profiles under galvanostatic charge/discharge between 0 V and 3.2 V at different specific currents (I) of a) PP-AC-EDLC, b) ACT-EDLC and c) ACT-EDLC-2, d) Ragone plots, and e) trend of the percentage of the capacitance normalized to the initial value (C_i/C_0 %) at 1 A g^{-1}. The total composite electrode mass loading was 11.6 mg cm^{-2} and 9.3 mg cm^{-2} for PP-AC-EDLC and ACT-EDLC (with 20 % binder), and it was 13.8 mg cm^{-2} for the ACT-EDLC-2 that featured (with 10% binder).

Conclusion

For the first time we demonstrated that pullulan can be used to design the major components (binder and separator) of green supercapacitors. The biomass derived PP-AC carbon features good capacitive behaviour in the EMIMTFSI IL with a specific capacitance of 115 F g^{-1}. Combining the good binding properties of pullulan-glycerol blends with the adequate mechanical properties of the electrospun fibers of pullulan mats and the electrochemical performance of the PP-AC carbon electrodes brings about EDLCs featuring up to 20 F g^{-1}, 5 kW kg^{-1} and 25 Wh kg^{-1} at 3.2 V. The IL is herein used not only for its good electrochemical properties in terms of stability and conductivity, but also because of its hydrophobicity, which enables the development of a novel concept of an end-of-life management of the EDLC. Indeed, it can be easily separated from the water soluble, bio-degradable polymer, from the carbons and current collectors by a simple immersion of the cell in water.

Therefore, our work paves the way towards the design of biodegradable, easy-to-recycle and disposable EDLCs.

Acknowledgments

The research has been carried out under the Italy-South Africa joint Research Programme 2018-2020 of the Italian Ministers of Foreign Affairs and of the Environment.

References

[1] M.M. Archuleta, Toxicity of materials used in the manufacture of lithium batteries, J. Power Sources 54 (1995) 138–142.

[2] K.M. Winslow, S.J. Laux, T.G. Townsend, A review on the growing concern and potential management strategies of waste lithium-ion batteries, Resour. Conserv. Recycl. 129 (2018) 263–277

[3] B. Dyatkin, V. Presser, M. Heon, M. R. Lukatskaya, M. Beidaghi, Y. Gogotsi, ChemSusChem, 6 (2013) 2269 -2280.

[4] M. Sevilla, A.B. Fuertes, A Green Approach to High-Performance Supercapacitor Electrodes: The Chemical Activation of Hydrochar with Potassium Bicarbonate, ChemSusChem. 9 (2016) 1880–1888.

[5] W. Zhao, L. Luo, X. Wu, T. Chen, Z. Li, Z. Zhang, et al., Facile and low-cost heteroatom-doped activated biocarbons derived from fir bark for electrochemical capacitors, Wood Sci. Technol. (2018).

[6] R. Thangavel, A.G. Kannan, R. Ponraj, V. Thangavel, D.W. Kim, Y.S. Lee, High-energy green supercapacitor driven by ionic liquid electrolytes as an ultra-high stable next-generation energy storage device, J. Power Sources. 383 (2018) 102–109.

[7] K.S. Sulaiman, A. Mat, A.K. Arof, Activated carbon from coconut leaves for electrical double-layer capacitor, Ionics (Kiel). 22 (2016) 911–918.

[8] S. Koutcheiko, V. Vorontsov, Activated carbon derived from wood biochar and its application in supercapacitors, J. Biobased Mater. Bioenergy. 7 (2013) 733–740.

[9] A. Jain, C. Xu, S. Jayaraman, R. Balasubramanian, J.Y.Y. Lee, M.P.P. Srinivasan, Mesoporous activated carbons with enhanced porosity by optimal hydrothermal pre-treatment of biomass for supercapacitor applications, Microporous Mesoporous Mater. 218 (2015) 55–61.

[10] M. Seredych, M. Koscinski, M. Sliwinska-Bartkowiak, T.J. Bandosz, Active pore space

utilization in nanoporous carbon-based supercapacitors: Effects of conductivity and pore accessibility, J. Power Sources. 220 (2012) 243–252.

[11] B. Hu, L. Bin Kong, L. Kang, K. Yan, T. Zhang, K. Li, et al., Synthesis of a hierarchical nanoporous carbon material with controllable pore size and effective surface area for high-performance electrochemical capacitors, RSC Adv. 7 (2017) 14516–14527.

[12] Y. Wang, Z. Zhao, W. Song, Z. Wang, X. Wu, From biological waste to honeycomb-like porous carbon for high energy density supercapacitor, J. Mater. Sci. (2018).

[13] F. Ochai-Ejeh, M.J. Madito, K. Makgopa, M.N. Rantho, O. Olaniyan, N. Manyala, Electrochemical performance of hybrid supercapacitor device based on birnessite-type manganese oxide decorated on uncapped carbon nanotubes and porous activated carbon nanostructures, Electrochim. Acta. 289 (2018) 363–375.

[14] Q. Abbas, P. Ratajczak, P. Babuchowska, A.L. Comte, D. Belanger, T. Brousse, et al., Strategies to Improve the Performance of Carbon/Carbon Capacitors in Salt Aqueous Electrolytes, J. Electrochem. Soc. 162 (2015) A5148–A5157.

[15] A. Bello, D.Y.Y. Momodu, M.J.J. Madito, K. Makgopa, K.M.M. Rambau, J.K.K. Dangbegnon, et al., Influence of $K_3Fe(CN)_6$ on the electrochemical performance of carbon derived from waste tyres by K_2CO_3 activation, Mater. Chem. Phys. 209 (2018) 262–270.

[16] K. Fic, M. Meller, J. Menzel, E. Frackowiak, Around the thermodynamic limitations of supercapacitors operating in aqueous electrolytes, Electrochim. Acta. 206 (2016) 496–503.

[17] D. Bresser, D. Buchholz, A. Moretti, A. Varzi, S. Passerini, Alternative binders for sustainable electrochemical energy storage–the transition to aqueous electrode processing and bio-derived polymers, Energy & Environ. Sci., 11 (2018) 3096-3127.

[18] K. C. Cheng, A. Demirci, J. M. Catchmark, Pullulan: biosynthesis, production, and applications, Appl. microbiology. and biotech., 92 (2011) 29.

[19] P. R. Vuddanda, M. Montenegro-Nicolini, J. O. Morales, S Velaga, Effect of plasticizers on the physico-mechanical properties of pullulan based pharmaceutical oral films, European J. Pharm. Sci., 96 (2017) 290-298.

[20] Q. Tong, Q. Xiao, L.-T. Lim, Preparation and properties of pullulan–alginate–carboxymethylcellulose blend films, Food Res. Int. 41 (2008) 1007–1014.

[21] S. Chen, S. He, H. Hou, Electrospinning technology for applications in supercapacitors. Current Org. Chem., 17 (2013) 1402-1410.

[22]D. Momodu, N.F. Sylla, B. Mutuma, A. Bello, T. Masikhwa, S. Lindberg, et al., Stable ionic-liquid-based symmetric supercapacitors from Capsicum seed porous carbons, J. Electroanal. Chem. 838 (2019) 119–128.

[23] M. Lazzari, M. Mastragostino, F. Soavi, Capacitance response of carbons in solvent-free ionic liquid electrolytes, Electrochem. Comm., 9 (2007) 1567-1572.

[24] M. Mastragostino, F. Soavi, Electrochemical Capacitors: Ionic Liquid Electrolytes. In: Juergen Garche, Chris Dyer, Patrick Moseley, Zempachi Ogumi, David Rand and Bruno Scrosati, editors. Encyclopedia of Electrochemical Power Sources, Vol 1. Amsterdam: Elsevier; 2009. pp. 649–657

[25] M. Lazzari, C. Arbizzani, F. Soavi, M. Mastragostino, EDLCs Based on Solvent-free Ionic Liquids, in Supercapacitors - Materials, Systems and Applications, F. Beguin and E. Frackowiak Eds., Wiley-VCH Verlag GmbH &Co. KGaA, Weinheim, p. 289-306, 2013, ISBN 978-3-527-32883-3

[26] J.C. Groen, L.A. Peffer, J. Pérez-Ramírez, Pore size determination in modified micro- and mesoporous materials. Pitfalls and limitations in gas adsorption data analysis, Microporous Mesoporous Mater. 60 (2003) 1–17.

[27] P.A. Webb, C. Orr, Analytical Methods in Fine Particle Technology, Micromeritics Instrument Corp., Norcross, 1997

[28] M. Lazzari, F. Soavi, M. Mastragostino, Mesoporous Carbon Design for Ionic Liquid-Based, Double-Layer Supercapacitors, Fuel Cells, 10(5) (2010) 840-847.

[29] M. Lazzari, M. Mastragostino, A. G. Pandolfo, V. Ruiz, F. Soavi, Role of carbon porosity and ion size in the development of ionic liquid-based supercapacitors, J. Electrochem. Soc., 158(1) (2011) A22-A25.

[30] C. Largeot, C. Portet ,J. Chmiola,P.L. Taberna, Y. Gogotsi,P. Simon, Relation between the ion size and pore size for an electric double-layer capacitor. J. Am. Chem. Soc., *130* (9) (2008), 2730-2731.

[31] M.A. Pimenta, G. Dresselhaus, M.S. Dresselhaus, L.G. Cançado, A. Jorio, R. Saito, Studying disorder in graphite-based systems by Raman spectroscopy, Phys. Chem. Chem. Phys. 9 (2007) 1276–1290.

[32] A. Sadezky, H. Muckenhuber, H. Grothe, R. Niessner, U. Pöschl, Raman microspectroscopy of soot and related carbonaceous materials: Spectral analysis and structural information, Carbon N. Y. 43 (2005) 1731–1742.

[33] J. Díaz, G. Paolicelli, S. Ferrer, F. Comin, Separation of the sp3 and sp2 components in the C1*s* photoemission spectra of amorphous carbon films, Phys. Rev. B. 54 (1996) 8064–8069.

[34] X.-L. Su, J.-R. Chen, G.-P. Zheng, J.-H. Yang, X.-X. Guan, P. Liu, et al., Three-dimensional porous activated carbon derived from loofah sponge biomass for supercapacitor applications, Appl. Surf. Sci. 436 (2018) 327–336

[35] D. Rosenthal, M. Ruta, R. Schlögl, L. Kiwi-Minsker, Combined XPS and TPD study of oxygen-functionalized carbon nanofibers grown on sintered metal fibers, Carbon N. Y. 48 (2010) 1835–1843.

[36] J.-W. Lu, Z.P. Zhang, X.Z. Ren, Y.Z. Chen, J. Yu, Z.X. Guo, High-elongation fiber mats by electrospinning of polyoxymethylene, Macromolecules 41 (2008) 3762–3764

[37] O. Barbieri, M. Hahn, A. Herzog, R. Kötz, Capacitance limits of high surface area activated carbons for double layer capacitors. Carbon, 43(6) (2005) 1303-1310.

[38] Bard, Allen J., et al. Electrochemical methods: fundamentals and applications. Vol. 2. New York: wiley, 1980.

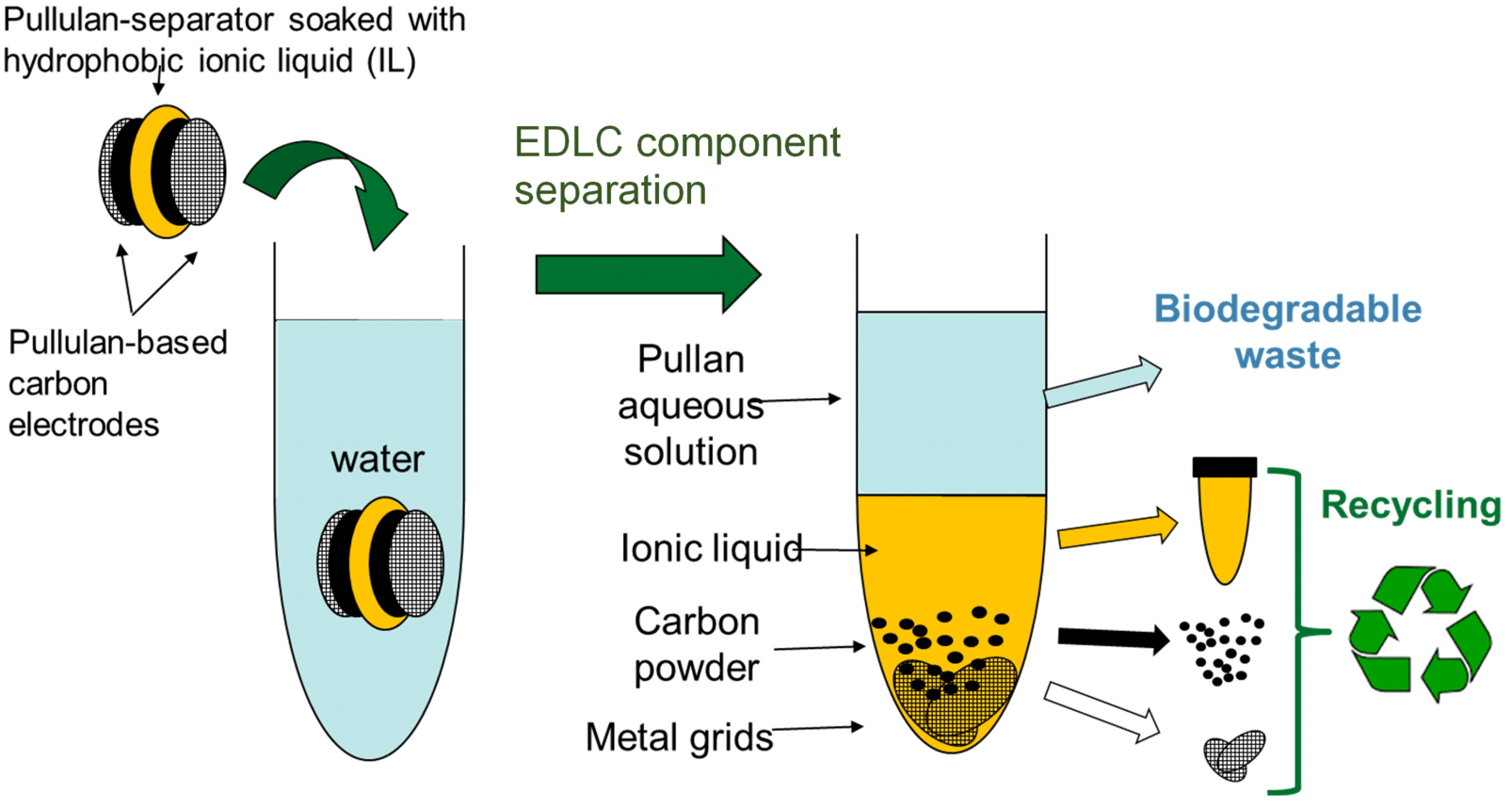
Pullulan-separator soaked with hydrophobic ionic liquid (IL)
Pullulan-based carbon electrodes
water
EDLC component separation
Pullan aqueous solution
Ionic liquid
Carbon powder
Metal grids
Biodegradable waste
Recycling

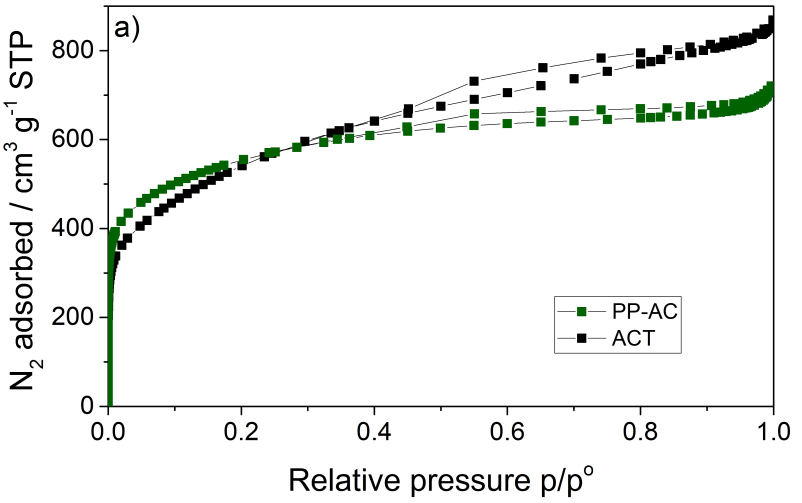
a)
N2 adsorbed / cm3 g-1 STP
Relative pressure p/p°
PP-AC
ACT

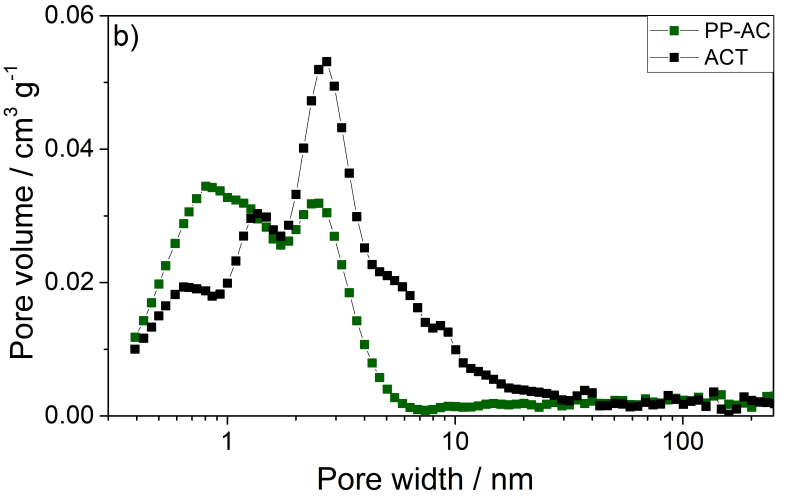
b)
Pore volume / cm3 g-1
Pore width / nm
PP-AC
ACT

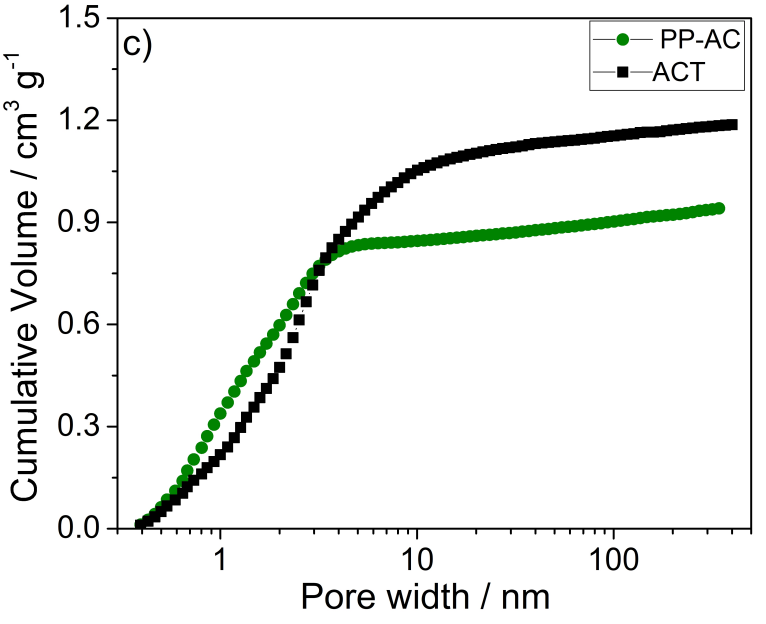
c)
Cumulative Volume / cm3 g-1
Pore width / nm
PP-AC
ACT

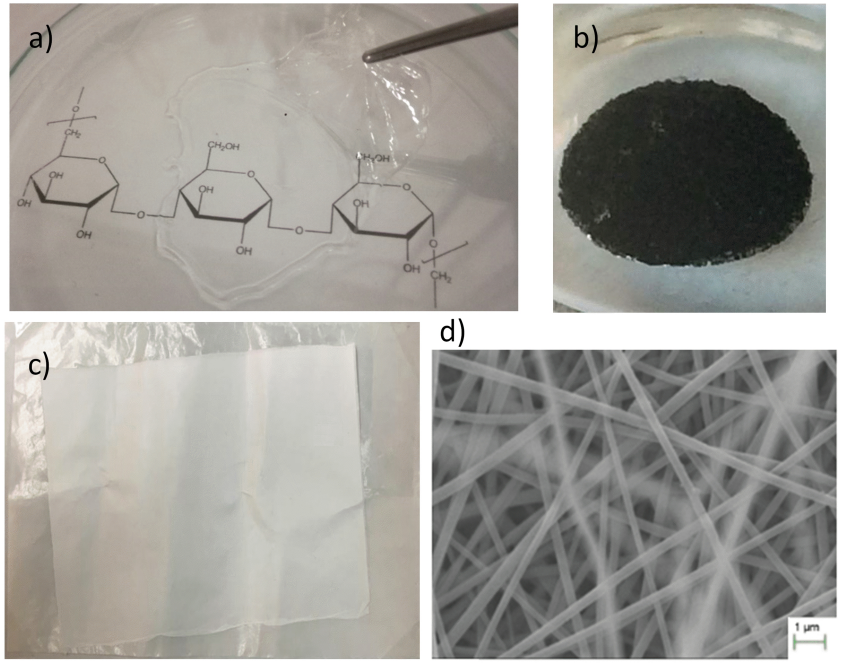
a)
b)
c)
d)
1 µm

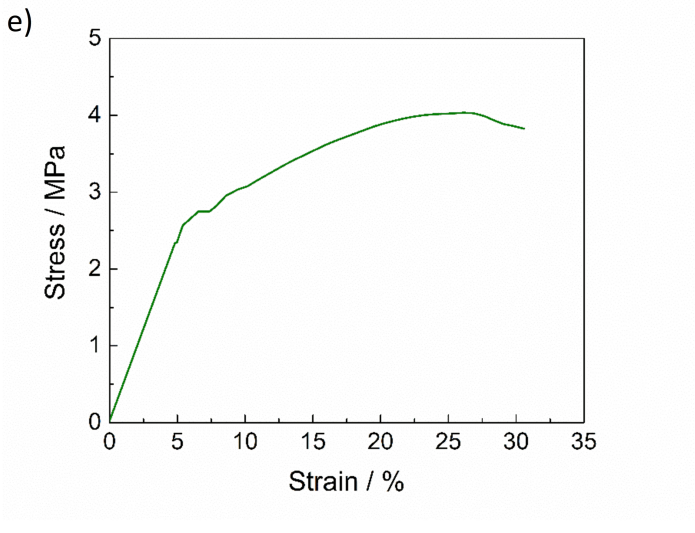
e)
Stress / MPa
Strain / %
0
1
2
3
4
5
0
5
10
15
20
25
30
35

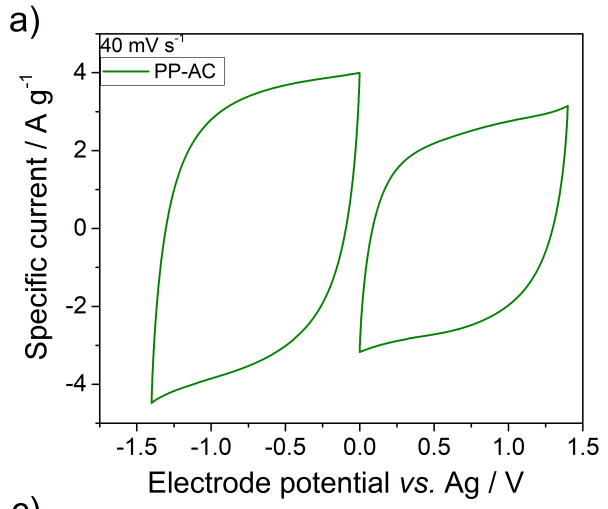
a)
40 mV s-1
PP-AC
Specific current / A g-1
Electrode potential vs. Ag / V

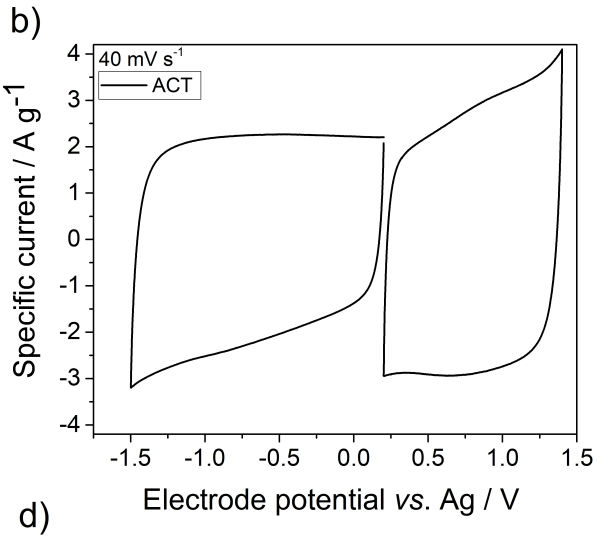
b)
40 mV s-1
ACT
Specific current / A g-1
Electrode potential vs. Ag / V

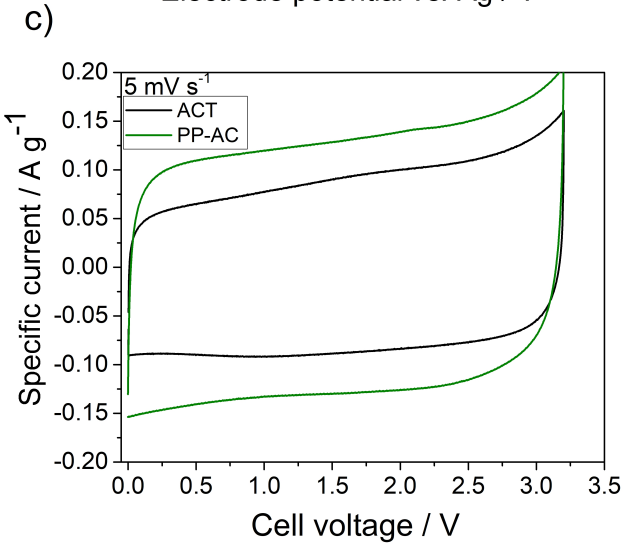
c)
5 mV s-1
ACT
PP-AC
Specific current / A g-1
Cell voltage / V

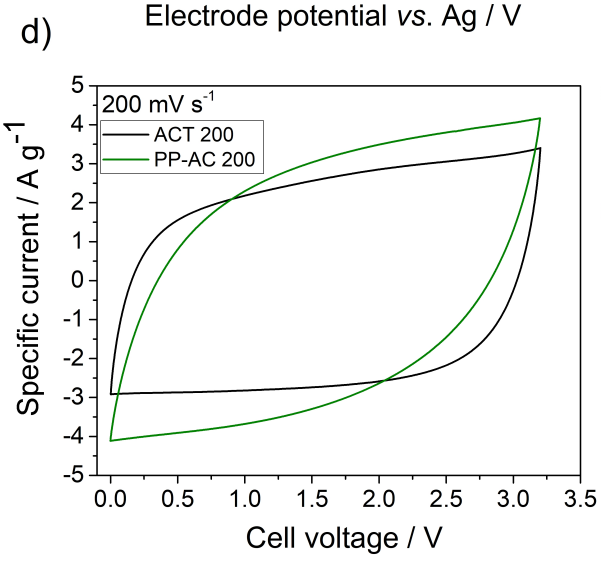
d)
200 mV s-1
ACT 200
PP-AC 200
Specific current / A g-1
Cell voltage / V

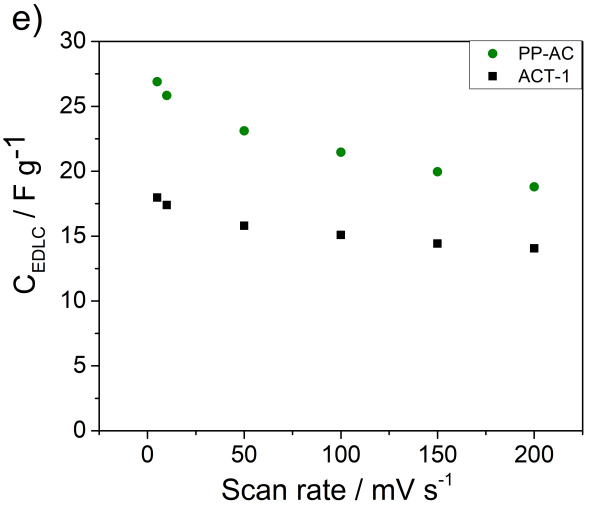
e)
PP-AC
ACT-1
C EDLC / F g-1
Scan rate / mV s-1

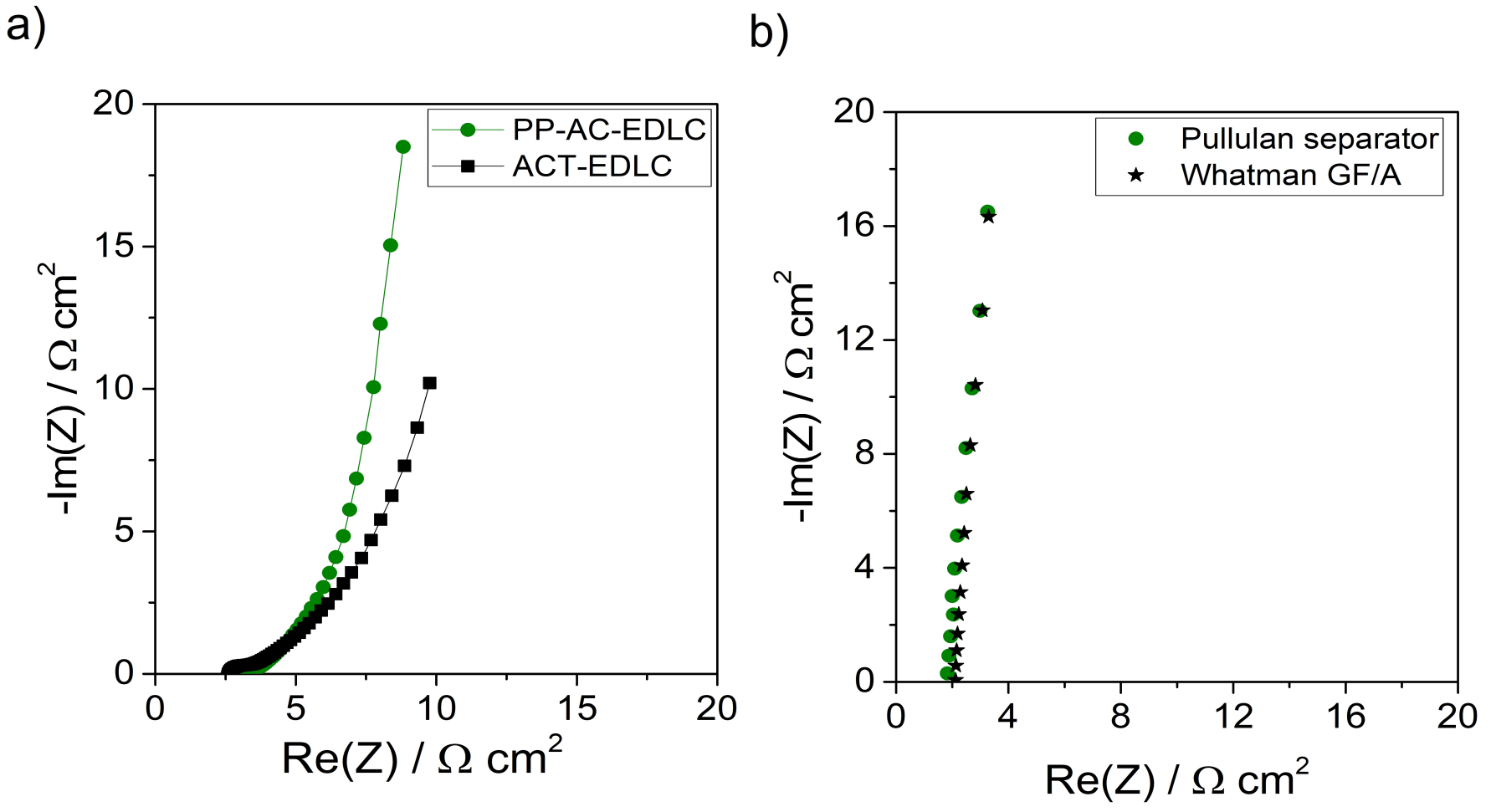
a)
b)
PP-AC-EDLC
ACT-EDLC
Pullulan separator
Whatman GF/A
-Im(Z) / Ω cm2
Re(Z) / Ω cm2
0
5
10
15
20
4
8
12
16

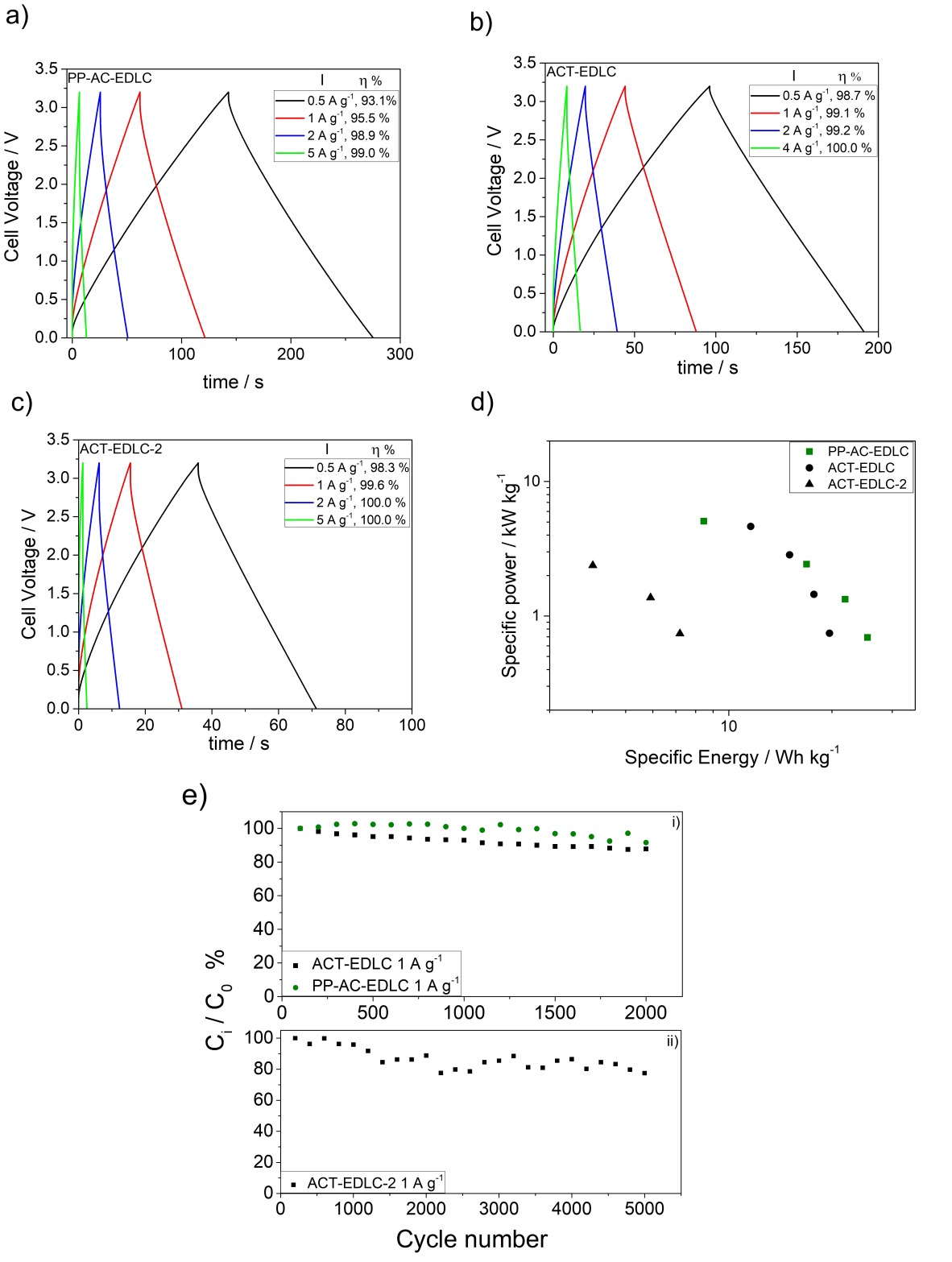
a)
PP-AC-EDLC
I η %
0.5 A g-1, 93.1%
1 A g-1, 95.5 %
2 A g-1, 98.9 %
5 A g-1, 99.0 %
Cell Voltage / V
time / s
b)
ACT-EDLC
I η %
0.5 A g-1, 98.7 %
1 A g-1, 99.1 %
2 A g-1, 99.2 %
4 A g-1, 100.0 %
Cell Voltage / V
time / s
c)
ACT-EDLC-2
I η %
0.5 A g-1, 98.3 %
1 A g-1, 99.6 %
2 A g-1, 100.0 %
5 A g-1, 100.0 %
Cell Voltage / V
time / s
d)
PP-AC-EDLC
ACT-EDLC
ACT-EDLC-2
Specific power / kW kg-1
Specific Energy / Wh kg-1
e)
i)
ACT-EDLC 1 A g-1
PP-AC-EDLC 1 A g-1
ii)
ACT-EDLC-2 1 A g-1
Ci / C0 %
Cycle number

Table 1. BET surface area (S_{BET}), DFT specific pore volume from pores with size > 0.4 nm ($V_{>0.4\ nm}$) of the PP-AC and ACT and specific capacitance (C_{carbon}) of the carbons from CVs at 40 mVs^{-1} in EMIMTFSI (average of the values of the positive and negative electrodes and normalized to the high surface area carbons, (i.e. excluding carbon black and binder). I_D/I_G is the ration of the Raman D-band and G-band intensities from [22, 23].

Carbon	Code	S_{BET} /m^2g^{-1}	$V_{>0.4\ nm}$ /cm^3g^{-1}	C_{carbon}/Fg^{-1}	I_D/I_G
Pepper-derived	PP-AC	1990	0.94	115	0.96
Commercial	ACT	1960	1.19	75	1.09